Bull. Mater. Sci. (2019) 42:62
https://doi.org/10.1007/s12034-019-1739-y

Prediction of magnetic and magnetocaloric properties in $Pr_{0.8-x}Bi_xSr_{0.2}MnO_3$ ($x = 0$, 0.05 and 0.1) manganites

A BEN JAZIA KHARRAT[1,*], E K HLIL[2] and W BOUJELBEN[1]

[1]Laboratoire de Physique des Matériaux, Faculté des Sciences de Sfax, Université de Sfax, 3000 Sfax, BP 1171, Tunisia
[2]Institut Néel, CNRS-Université J. Fourier, 38042 Grenoble, BP 166, France
*Author for correspondence (benjaziaaida@gmail.com)

MS received 9 May 2018; accepted 2 August 2018; published online 6 March 2019

Abstract. In this work, we have investigated the magnetic and magnetocaloric properties of $Pr_{0.8-x}Bi_xSr_{0.2}MnO_3$ ($x = 0$, 0.05 and 0.1) polycrystalline manganites prepared by sol–gel route on the basis of a phenomenological model. Temperature dependence of magnetization indicates that all our samples exhibit a second order paramagnetic to ferromagnetic transition with a decrease in temperature. A correlation between experimental results and theoretical analysis based on a phenomenological model is investigated. The magnetic and magnetocaloric measurements are well simulated by this model. Under a magnetic applied field of 5 T, the theoretical absolute values of the maximum of magnetic entropy change ΔS_{Max} are found to be equal to 5.33, 3.33 and 2.97 J kg^{-1} K^{-1} for $x = 0$, 0.05 and 0.1 respectively. The relative cooling power and the specific heat capacity values are also estimated. The predicted results permit us to conclude that our compounds may be promising candidates for magnetic refrigeration at low temperatures.

Keywords. Magnetic transition; phenomenological model; magnetocaloric effect; critical exponents; specific heat.

1. Introduction

In recent years, magnetic materials with a high magnetocaloric effect (MCE) have been investigated to provide an alternative to the conventional vapour-cycle refrigeration in particular at room temperature [1–3]. Magnetic refrigeration techniques based on these friendly environmental compounds are based on the alignment of randomly oriented magnetic moments by simply applying an external magnetic field. This effect yields to the heating of the material and the created energy can be transferred to the ambient atmosphere. Conversely, in the demagnetization process, the magnetic moments randomize again leading to the cooling of the studied compound. Many materials with high MCE such as gadolinium (Gd), $Er_{12}Co_7$, $Gd_5(Si_2Ge_2)$, $LaFe_{11.4}Si_{1.6}$, $Ho_{12}Co_7$ [4–8] have been reported in the literature. Manganites with the general formula $R_{1-x}A_xMnO_3$ (R is a rare earth element and A is a divalent alkaline earth element) are considered nowadays as excellent candidates for magnetic refrigeration owing to their high magnetic performance in addition to their low cost and ease of preparation [9]. In our laboratory, the substitution of diamagnetic bismuth in the A-site or B-site of manganites has been studied [10–12]. The obtained results have demonstrated that the physical properties of these compounds are strongly affected.

In a previous report [10], we have studied the effect of Bi doping on the critical behaviour and magnetocaloric properties of $Pr_{0.8-x}Bi_xSr_{0.2}MnO_3$ ($x = 0$, 0.05 and 0.1) materials prepared by a sol–gel route. We have demonstrated that around T_C (estimated at 210, 155 and 140 K for $x = 0$, 0.05 and 0.1, respectively) and for an applied magnetic field of 5 T, $|\Delta S_M|$ decreases from 5.41 J kg^{-1} K^{-1} for $x = 0$ to 3.11 J kg^{-1} K^{-1} for $x = 0.1$, respectively. The most interesting result is that as compared with the parent sample, $|\Delta S_M|$ for doped samples exhibits a large broad variation with temperature around T_C giving rise to important relative cooling power (RCP). The modellization of the magnetocaloric properties of these materials may give us a deep understanding of the evolution of magnetic entropy change with the applied magnetic field.

For a magnetic material with a ferromagnetic (FM) to paramagnetic (PM) transition, a phenomenological model proposed by Hamad [13] is widely used to simulate the temperature evolution of magnetization and to investigate the magnetocaloric properties, such as magnetic entropy change, the RCP and the heat-capacity change [14,15]. For a magnetic system with multiple magnetic transitions, Hsini *et al* [16] have used this phenomenological model to simulate the magnetocaloric results in the charge ordered $Pr_{0.5}Sr_{0.5}MnO_3$ manganite. Indeed, this compound exhibits two magnetic transitions: a first order antiferromagnetic to a FM transition at T_N around 165 K followed by a second order FM to PM at $T_C = 255$ K [17]. A good agreement is obtained between the simulated magnetization $M(T)$ and the magnetic entropy change data with the simulated results at a low applied magnetic field $\mu_0 H = 0.05$ T confirming the usefulness of the phenomenological theory proposed by Hamad [13] for the study of magnetic systems with multiple magnetic transitions.

In this paper, we have used the phenomenological model to simulate experimental results and predict the magnetic and magnetocaloric properties of the $Pr_{0.8-x}Bi_xSr_{0.2}MnO_3$ ($x = 0$, 0.05 and 0.1) compounds. We focus our interest on the magnetic entropy change ΔS_M, the RCP and the specific heat change $\Delta C_p(T, \mu_0 H)$. The critical exponents were determined and compared to those determined in our previous work [10].

2. Experimental

Our compounds were prepared using the sol–gel process using high purity Pr_6O_{11}, Bi_2O_3, $SrCo_3$ and MnO_2 precursors. Details of the experimental conditions were explained in our previous work [18]. Structural quality of the samples was confirmed by the X-ray diffraction (XRD) measurements at room temperature. The refinement of the XRD patterns with the Rietveld technique using Fullprof software has indicated that our samples crystallize in the orthorhombic structure with the *Pnma* space group. The magnetic measurements were carried out using a vibrating sample magnetometer in the temperature range of 5–330 K and under applied magnetic fields up to 5 T.

3. Theoretical considerations

The phenomenological model adopted in this study is based on Hamad's [13] work. In this approach, the temperature evolution of magnetization is given by:

$$M(T) = \frac{(M_i - M_f)}{2}\tanh[a(T_C - T)] + bT + c, \quad (1)$$

where

1. M_i and M_f are respectively the initial and the final magnetizations at FM to PM transition as illustrated in figure 1.

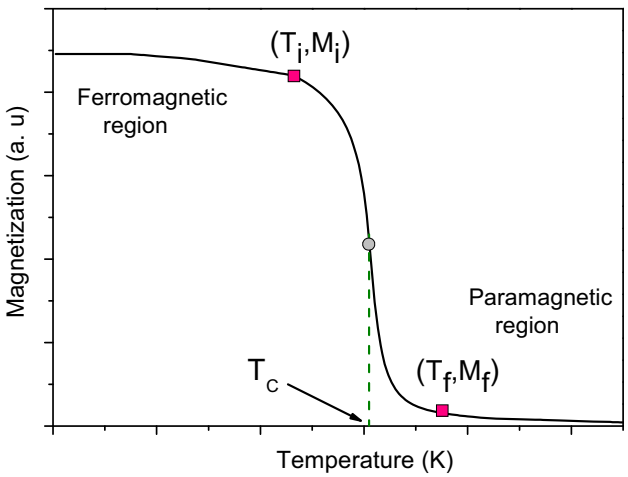

Figure 1. Temperature dependence of the magnetization (M) under constant applied magnetic field.

2. b is the magnetization sensitivity in the FM region before transition ($b = dM/dT$).
3. $c = (M_i + M_f)/2 - b * T_C$.
4. $a = 2(b - S_C)/(M_i - M_f)$, S_C is the magnetization sensitivity (dM/dT) at Curie temperature, T_C.

The magnetic entropy change which results from spin ordering under isothermal magnetic field change from 0 to $\mu_0 H_{max}$, can be determined using the phenomenological model given by the following expression [19]:

$$\Delta S_M(T) = \left\{-a\frac{(M_i - M_f)}{2}\text{sech}^2[a(T_C - T)] + b\right\}\mu_0 H_{max}, \quad (2)$$

where $\text{sech}(x) = 1/\cosh(x)$.

As is known, $\Delta S_M(T)$ reaches its maximum value ΔS_{Max} at Curie temperature T_C which can be evaluated as the following expression [20]:

$$\Delta S_{Max} = \left[-a\frac{(M_i - M_f)}{2} + b\right]\mu_0 H_{max}. \quad (3)$$

The full width at half maximum δT_{FWHM} can be written as [19, 20]:

$$\delta T_{FWHM} = \frac{2}{a}\text{sech}\left[\sqrt{\frac{2a\,(M_i - M_f)}{a\,(M_i - M_f) + 2b}}\right]. \quad (4)$$

The efficiency of any magnetic material can be evaluated using the RCP determined from equation (3) and (4):

$$\text{RCP} = -\Delta S_M(T, H_{Max})\delta T_{FWHM} = \left(M_i - M_f - 2\frac{b}{a}\right)\mu_0 H_{Max} \times \text{sech}\left[\sqrt{\frac{2a(M_i - M_f)}{a(M_i - M_f) + 2b}}\right]. \quad (5)$$

The heat capacity can be evaluated from the magnetic contribution to $\Delta S_M(T)$ by the following expression [21]:

$$\Delta C_p(T, \mu_0 H) = C_p(T, \mu_0 H) - C_p(T, 0) = T\frac{\partial[\Delta S_M(T, \mu_0 H)]}{\partial T}, \quad (6)$$

which can be written as [21,22]:

$$\Delta C_p(T, \mu_0 H) = -TA^2(M_i - M_f) \times \tanh[A(T_C - T)]\mu_0 H_{max}\text{sech}^2[A(T_C - T)]. \quad (7)$$

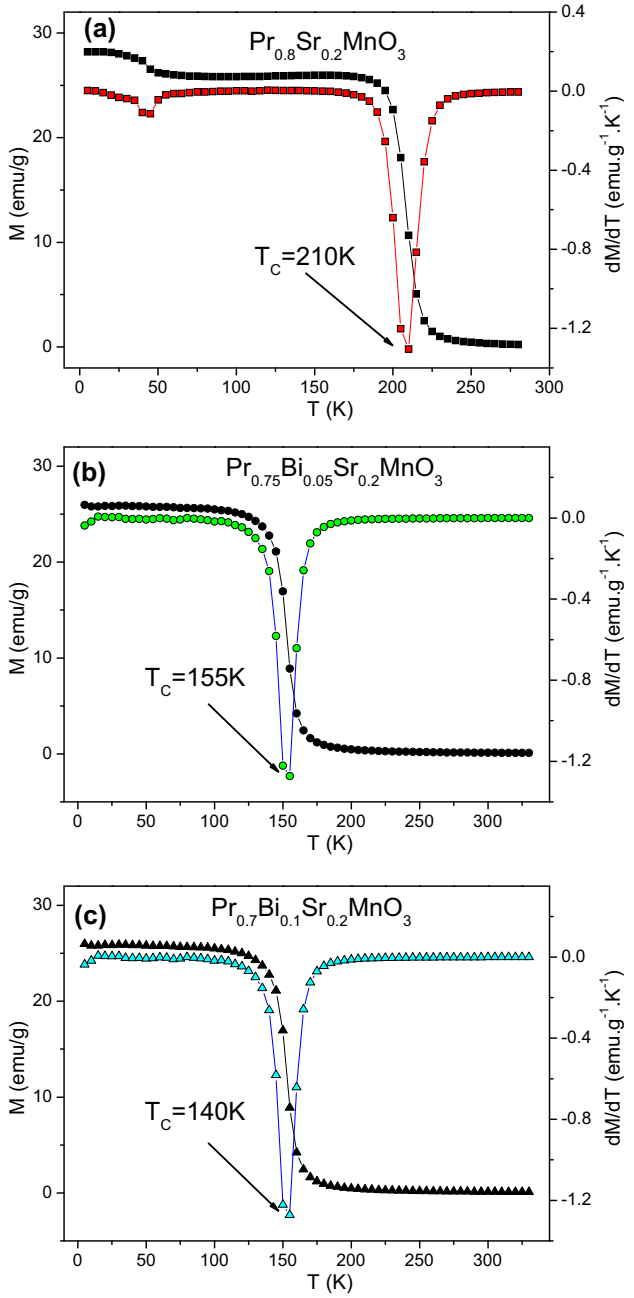

Figure 2. Temperature evolution of the magnetization $M(T)$ determined for the $Pr_{0.8-x}Bi_xSr_{0.2}MnO_3$ compounds under a magnetic applied field of 0.05 T: (**a**) $x = 0$, (**b**) $x = 0.05$ and (**c**) $x = 0.1$. The inset of each figure shows the evolution of dM/dT with temperature.

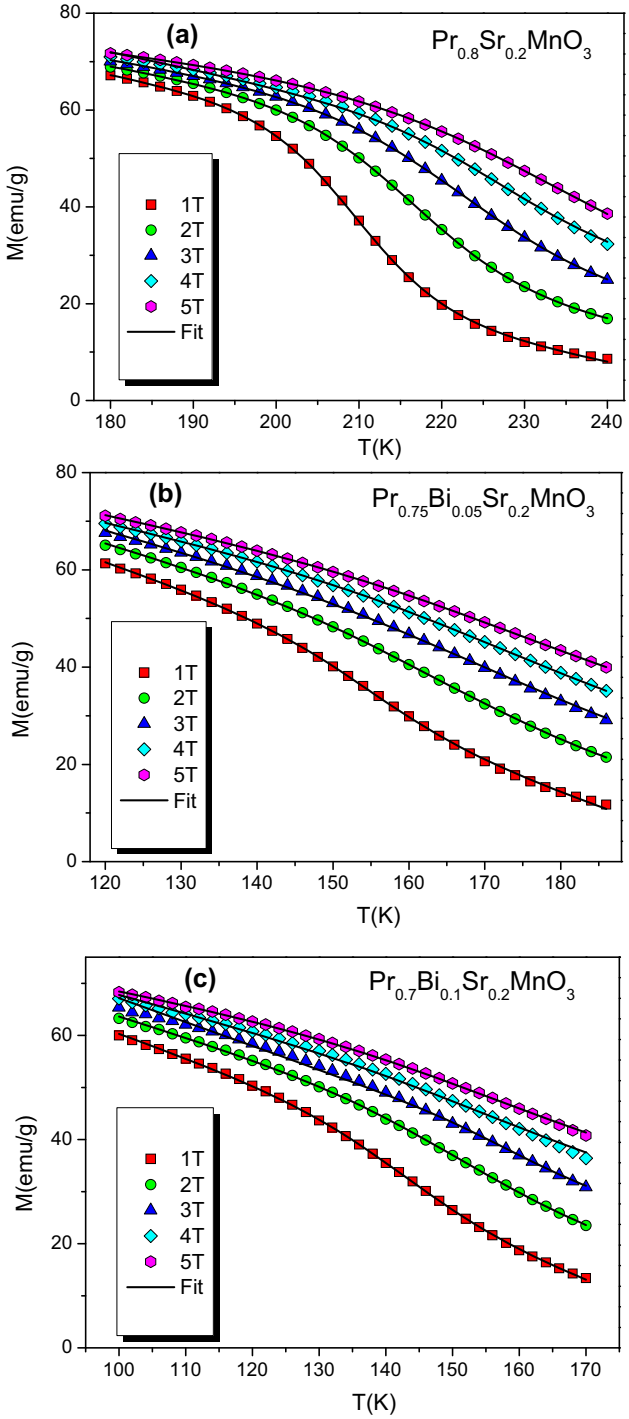

Figure 3. Temperature dependence of the magnetization at different magnetic applied fields for $Pr_{0.8-x}Bi_xSr_{0.2}MnO_3$ compounds ($x = 0$, 0.05 and 0.1). Symbols represent the experimental data and solid lines represent the simulated results.

4. Results and discussion

Magnetization dependence *vs*. temperature under an applied magnetic field of 0.05 T for the $Pr_{0.8-x}Bi_xSr_{0.2}MnO_3$ ($x = 0$, 0.05 and 0.1) samples are reported in figure 2. As seen, all compounds exhibit a PM to FM transition when the temperature decreases. From the dM/dT plots, we have determined the Curie temperature for each compound which are 210, 155 and 140 K for $x = 0$, 0.05 and 0.1, respectively. This step is important since it gives the adequate parameters necessary to fit the magnetization data. Figure 3 shows the temperature dependence of magnetization $M(T)$ under magnetic

Table 1. Parameters fit from equation (1) for the $Pr_{0.8-x}Bi_xSr_{0.2}MnO_3$ ($x = 0$, 0.05 and 0.1) compounds at different magnetic applied fields.

$\mu_0 H$ (T)	M_i (emu g^{-1})	M_f (emu g^{-1})	T_C (K)	b (emu g^{-1} K^{-1})	S_c (emu g^{-1} K^{-1})	R^2
			$Pr_{0.8}Sr_{0.2}MnO_3$			
1	57.258	18.250	209.64	−0.3393	−1.1408	1
2	58.384	22.533	216.62	−0.2952	−1.1105	1
3	58.824	25.728	222.63	−0.2754	−1.0121	1
4	55.354	33.838	227.09	−0.3533	−0.9034	1
5	61.381	26.684	233.80	−0.0819	−0.8902	1
			$Pr_{0.75}Bi_{0.05}Sr_{0.2}MnO_3$			
1	42.728	27.762	154.70	−0.5470	−0.9060	1
2	46.603	29.819	162.90	−0.4474	−0.8157	1
3	48.823	32.886	168.67	−0.4072	−0.6800	1
4	51.686	35.108	172.72	−0.3483	−0.6437	1
5	54.134	38.392	175.03	−0.3179	−0.5823	1
			$Pr_{0.7}Bi_{0.1}Sr_{0.2}MnO_3$			
1	40.793	24.717	143.02	−0.4510	−0.8193	1
2	42.862	29.040	150.79	−0.3923	−0.7384	1
3	43.792	36.380	154.95	−0.4527	−0.6473	1
4	48.567	40.146	156.62	−0.3506	−0.5064	1
5	55.020	41.162	157.44	−0.2441	−0.4796	1

applied fields up to 5 T. Using the values extracted from $M(T)$ at $\mu_0 H = 0.05$ T, we have simulated the experimental magnetization data $M(T)$ for different applied magnetic fields from 1 to 5 T using equation (1). The results are gathered in table 1. In figure 3, the symbols display the experimental data and the solid lines represent the simulated curves using the parameters shown in table 1. As seen, although our measurements were made around Curie temperature, a very good agreement between experimental and simulated data is obtained which indicates the accuracy of this method.

Using the values of table 1, we have calculated the temperature dependence of $(-\Delta S_M)$ at different magnetic applied fields according to equation (2). We have chosen to determine $(-\Delta S_M)$ for the same magnetic fields to compare the predicted values with those obtained in our previous work [10]. The results, plotted in figure 4, show a satisfied agreement between the experimental and theoretical data. In addition, the negative values of the magnetic entropy change obtained in the whole temperature of study, confirm the FM behaviour of our compounds [23]. It is important to note that the main advantage of the phenomenological model is that we can easily predict the magnetocaloric properties of the compound under any magnetic applied field. Our samples show a large magnetic entropy change which can be explained by the double-exchange mechanism between Mn^{3+} and Mn^{4+} ions proposed by Zener [24] which favours FM interactions due to the hopping of e_g electrons. Besides, in perovskite magnetic materials, the change in the magnetic entropy is induced by the coupling between the applied magnetic field and the magnetic sublattice which affects, in particular, the magnetic part of the total entropy due to the corresponding change in the magnetic field [25,26]. In addition, $\Delta S_M(T, \Delta H)$ is maximized near the magnetic ordering temperature (T_C) of the studied materials where the $M(T)$ curves change rapidly with temperature [4].

The magnetic field evolution of the maximum entropy change (around T_C) can be evaluated using the following power law [27]:

$$(-\Delta S_{Max}) = \alpha(\mu_0 H)^n, \tag{8}$$

where α is a constant and n depends on the magnetic state of the studied compounds. We have plotted in figure 5, the evolution of the theoretical values of $(-\Delta S_{Max})$ *vs.* $(\mu_0 H)$ as well as the fit by equation (8). The obtained values of the exponent n are 0.838, 0.98 and 1.016 for $x = 0$, 0.05 and 0.1, respectively. These values are in good agreement with those obtained from experimental data [10], but higher than those expected with the mean field theory [28]. The difference is usually attributed to the existence of inhomogeneities in the vicinity of T_C [10].

With the theoretical $(-\Delta S_M)$ values, we have plotted in figure 6, the magnetic field dependence of δ_{FWHM} and RCP relative to the $Pr_{0.8-x}Bi_xSr_{0.2}MnO_3$ ($x = 0$, 0.05 and 0.1) samples. As we can see, although doping with bismuth reduces the maximum entropy change, it causes the increase in δ_{FWHM} which is beneficial for magnetic refrigeration in the considered domain of applications. This broadening can be explained by the decrease of grain size estimated at 82, 62 and 37 nm for $x = 0$, 0.05 and 0.1, respectively

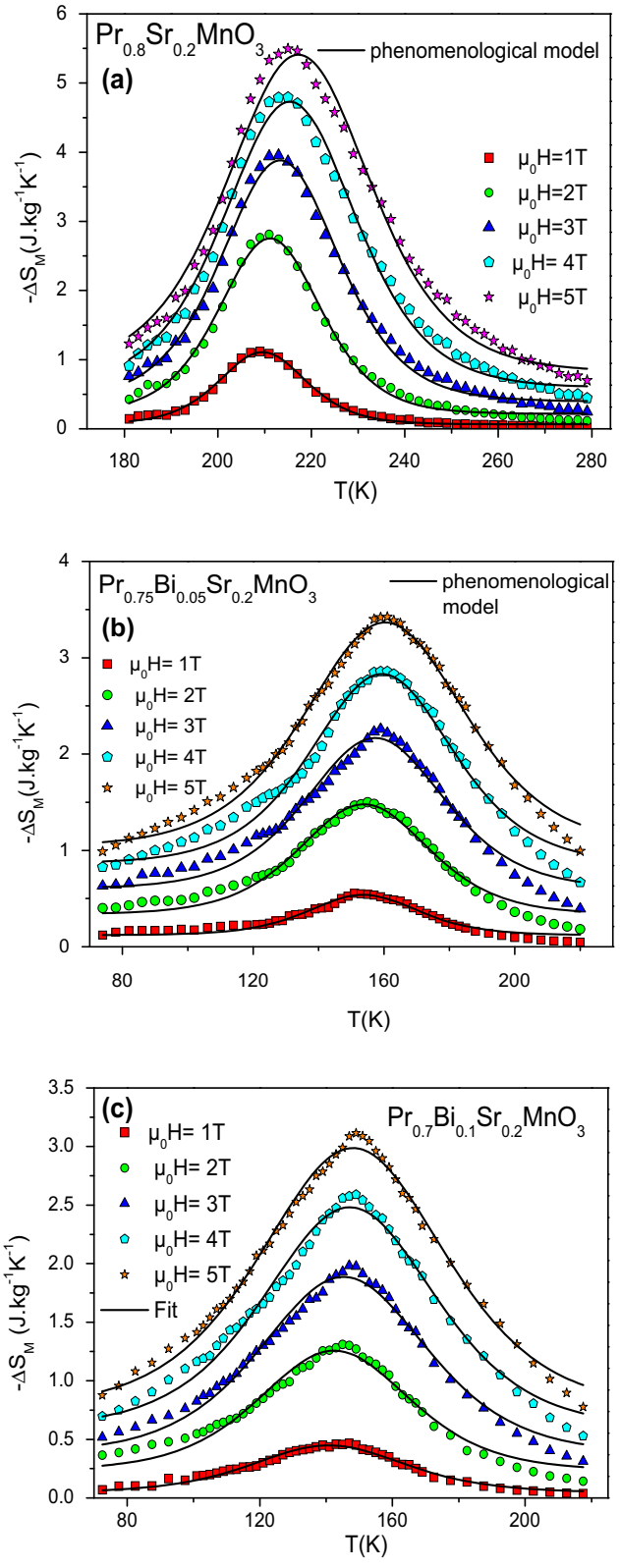

Figure 4. Temperature dependence of the magnetic entropy change $|\Delta S_{\mathrm{M}}(T)|$ under different magnetic applied fields for $Pr_{0.8-x}Bi_xSr_{0.2}MnO_3$ compounds (**a**) $x = 0$, (**b**) $x = 0.05$ and (**c**) $x = 0.1$. Solid lines show the predicted values of $|\Delta S_{\mathrm{M}}(T)|$ using table 1 and symbols represent the experimental data.

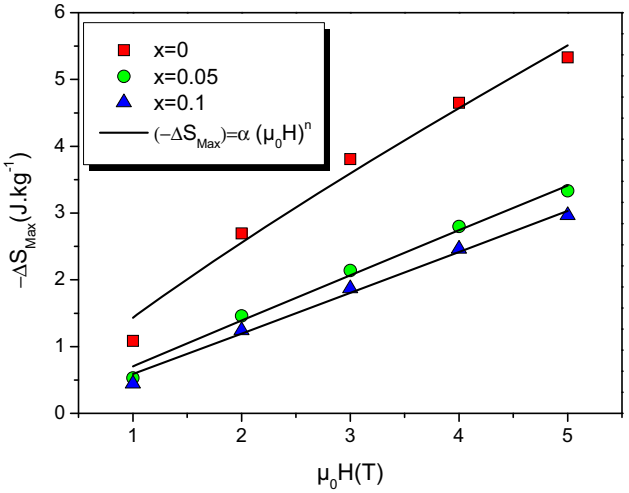

Figure 5. Magnetic field evolution of the maximum entropy change $|\Delta S_{\mathrm{Max}}|$ for $Pr_{0.8-x}Bi_xSr_{0.2}MnO_3$ ($x = 0$, 0.05 and 0.1) compounds.

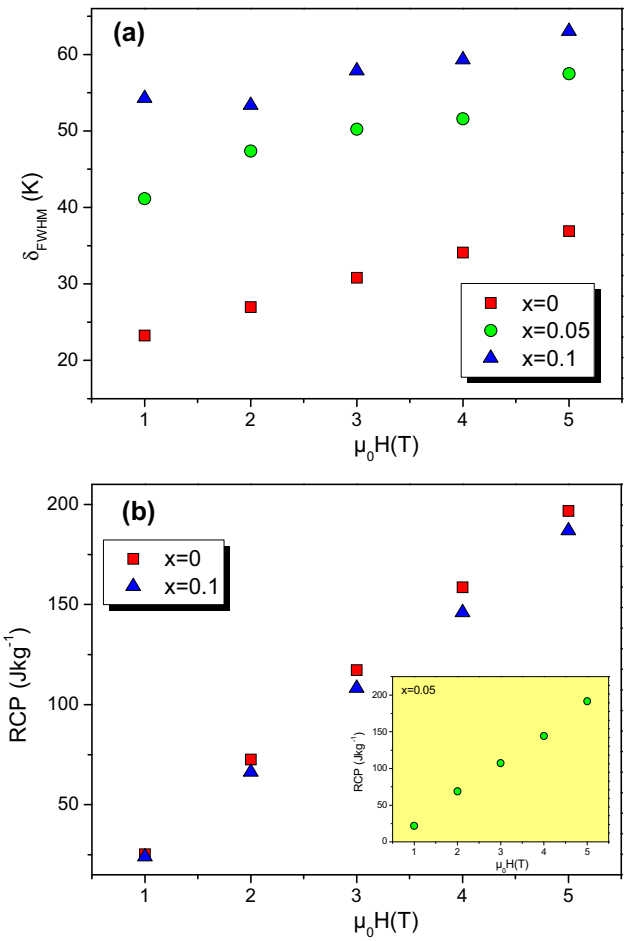

Figure 6. Evolution of (**a**) δ_{FWHM} and (**b**) RCP *vs*. magnetic field relative to the $Pr_{0.8-x}Bi_xSr_{0.2}MnO_3$ ($x = 0$, 0.05 and 0.1) compounds.

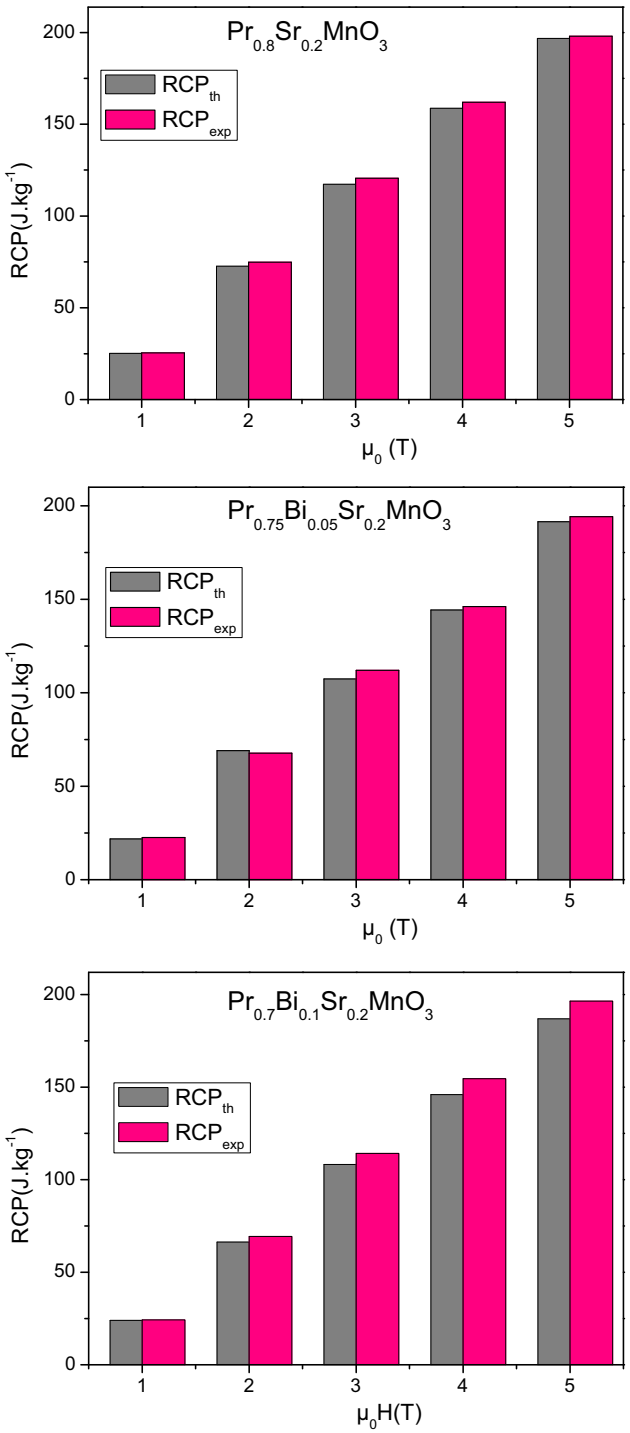

Figure 7. Comparison between RCP values obtained from the phenomenological model (RCP_{th}) and those obtained from experimental data (RCP_{exp}) for $Pr_{0.8-x}Bi_xSr_{0.2}MnO_3$ ($x = 0$, 0.05 and 0.1) compounds.

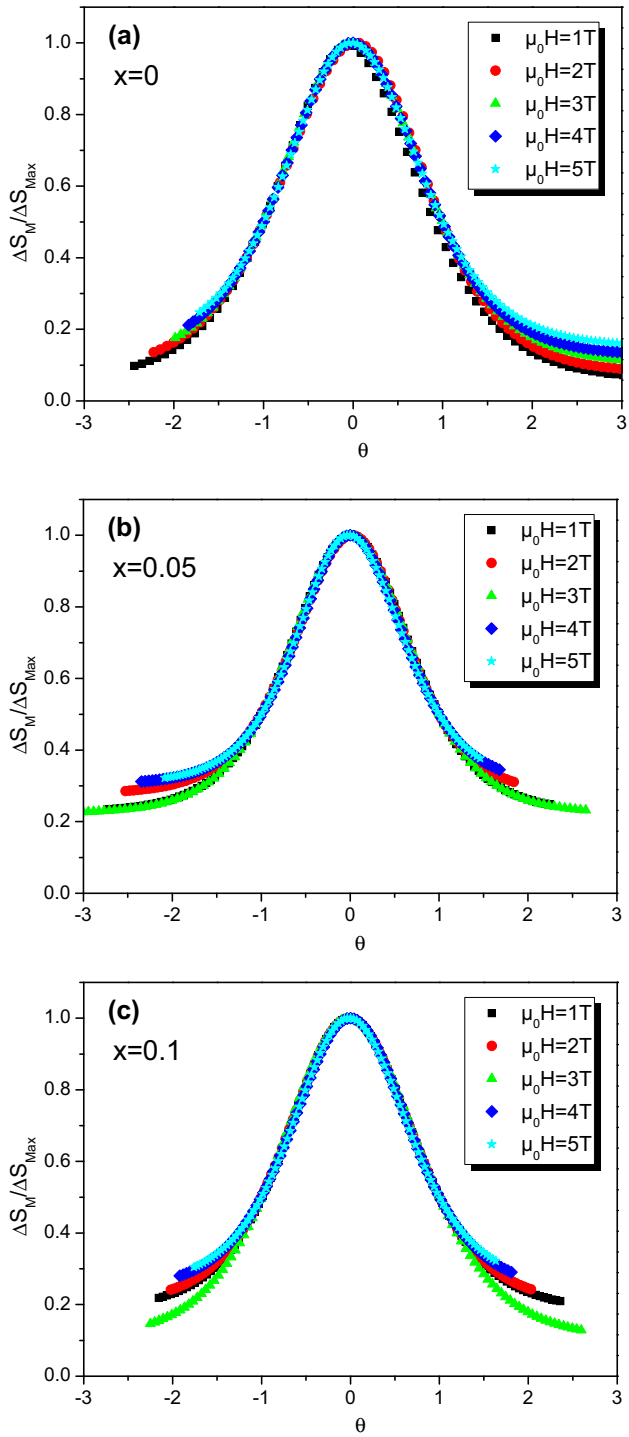

Figure 8. Normalized entropy change *vs*. rescaled temperature θ for $Pr_{0.8-x}Bi_xSr_{0.2}MnO_3$ ($x = 0$, 0.05 and 0.1) compounds at different applied magnetic fields.

[18]. Indeed, the decrease of the particle size induces larger surface-near spins which may have an FM coupling lower than that of bulk grains. As a result, a distribution of Curie temperature may occur and can be at the origin of the broadening of $|\Delta S_M|$.

In figure 7, we have compared the theoretical values of RCP, which is considered as the most important parameter to evaluate the MCE, obtained with the phenomenological model with those obtained from experimental data. The good agreement shows, once again, the efficiency of this method.

We can conclude that the RCP values can be directly predicted from $M(T)$ measurements.

On the other hand and according to Franco *et al* [29], a phenomenological universal curve can be determined by normalizing all $\Delta S_M(T)$ curves using their respective peak entropy change ($-\Delta S_{Max}$) and rescaling the temperature axis below and above Curie temperature T_C as defined in the following equation:

$$\theta = \begin{cases} -\dfrac{(T - T_C)}{(T_{r1} - T_C)}, & T \leq T_C, \\ \dfrac{(T - T_C)}{(T_{r2} - T_C)}, & T > T_C, \end{cases} \tag{9}$$

where θ is the rescaled temperature and T_{r1} and T_{r2} are the temperatures selected for $\Delta S_M = \Delta S_{Max}/2$. Figure 8 shows the evolution of the new constructed curves with θ values for different magnetic applied fields. As we can see, for each compound, all curves collapse into one universal curve confirming that the magnetic transition is a second-ordered phase transition.

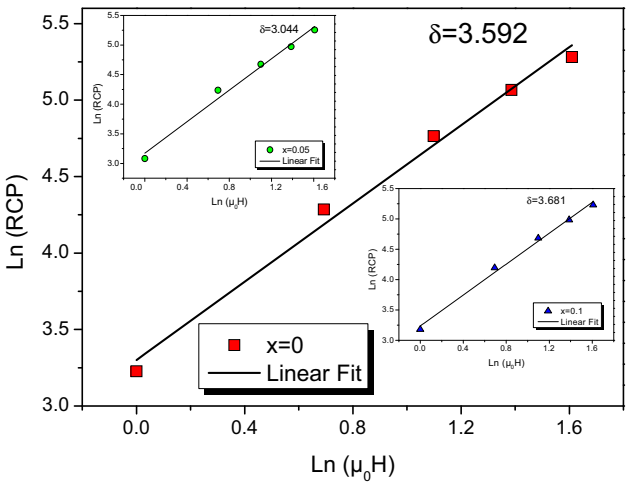

Figure 9. ln(RCP) *vs.* ln($\mu_0 H$) for $Pr_{0.8-x}Bi_xSr_{0.2}MnO_3$ ($x = 0$, 0.05 and 0.1) compounds.

Using the predicted values of RCP and the exponent n calculated from equations (5) and (8), respectively, we can determine the critical exponents characterizing the magnetic transition around Curie temperature defined as: γ is the isothermal magnetic susceptibility exponent, β is the spontaneous magnetization exponent and δ is the critical isotherm exponent. Indeed, the field dependence of RCP can be expressed by the following power law [29]:

$$\mathrm{RCP} = A(\mu_0 H)^{1+1/\delta}, \tag{10}$$

where A is a constant. For $T = T_C$, the n exponent calculated previously can be determined using the equation [30]:

$$n(T_C) = 1 + (\beta - 1)/(\beta + \gamma). \tag{11}$$

As the relation between β and γ exponents [31]: $\beta\gamma = (\beta + \gamma)$, equation (11) can be written as:

$$n(T_C) = 1 + \frac{1}{\delta}(1 - 1/\beta). \tag{12}$$

In figure 9, we have plotted ln(RCP) *vs.* ln($\mu_0 H$) for all our compounds to determine the critical exponent δ. Then, β and γ values can be calculated using equations (11) and (12). Results are summarized in table 2. A big discrepancy is obtained between the critical exponents determined from theoretical RCP values and those obtained experimentally from ref. [10]. We can conclude that the phenomenological model is not accurate to determine the critical exponents. On the other hand, we have calculated the temperature dependence of the specific heat using equation (7) for all our studied compounds. This method can be an alternative to experimental results. In figure 10, we have plotted the temperature dependence of the specific heat ΔC_p for different applied magnetic fields ($\mu_0 H = 1$, 2, 3, 4 and 5 T). As we can see, the evolution of the specific heat $\Delta C_p(T, \mu_0 H)$ deviates from zero only in the vicinity of the Curie temperature for all the studied samples. In addition, $\Delta C_p(T, \mu_0 H)$ values are negative below the transition temperature and are positive above the transition temperature. The estimated values of $\Delta C_{p,min}$ and

Table 2. Critical exponents determined theoretically from the phenomenological model and those obtained experimentally (and taken from ref. [10]) for the studied compounds.

Sample	n	δ	β	γ	Ref.
$Pr_{0.8}Sr_{0.2}MnO_3$	0.838	3.592	0.632	1.638	This work
$Pr_{0.75}Bi_{0.05}Sr_{0.2}MnO_3$	0.980	3.044	0.942	1.926	
$Pr_{0.7}Bi_{0.1}Sr_{0.2}MnO_3$	1.016	3.681	1.062	2.848	
$Pr_{0.8}Sr_{0.2}MnO_3$	0.818	4.81	0.260	0.993	[10]
$Pr_{0.75}Bi_{0.05}Sr_{0.2}MnO_3$	0.980	4.70	0.303	1.168	
$Pr_{0.7}Bi_{0.1}Sr_{0.2}MnO_3$	1.016	4.82	0.302	1.168	

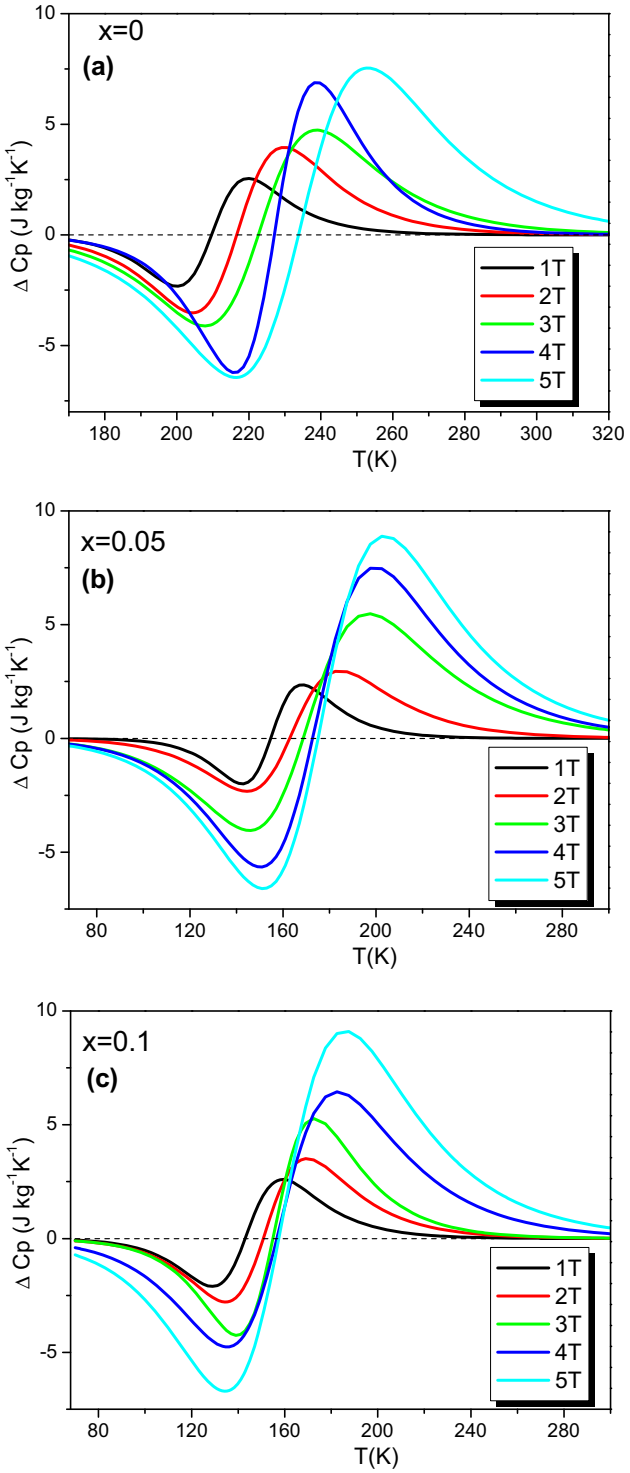

Figure 10. Temperature evolution of the predicted heat capacity under different magnetic applied fields for the $Pr_{0.8-x}Bi_xSr_{0.2}MnO_3$ ($x = 0$, 0.05 and 0.1) compounds.

$\Delta C_{p,max}$ at $\mu_0 H = 5$ T for all the samples that are shown in table 3. The obtained values show an increase with the increase of Bi-content which highlights the importance of this dopant in the $Pr_{0.8}Sr_{0.2}MnO_3$ compound. In addition, these results can be substantially interesting as compared to those obtained with materials suggested for magnetic refrigeration.

Table 3. Specific heat values obtained at $\mu_0 H = 5$ T for the $Pr_{0.8-x}Bi_xSr_{0.2}MnO_3$ (x=0, 0.05 and 0.1) compounds.

Sample	$\Delta C_{p,min}$ ($Jkg^{-1}K^{-1}$)	$\Delta C_{p,max}$ ($Jkg^{-1}K^{-1}$)
$Pr_{0.8}Sr_{0.2}MnO_3$	−6.438	7.541
$Pr_{0.75}Bi_{0.05}Sr_{0.2}MnO_3$	−6.600	8.888
$Pr_{0.7}Bi_{0.1}Sr_{0.2}MnO_3$	−6.704	9.101

5. Conclusion

High purity polycrystalline $Pr_{0.8-x}Bi_xSr_{0.2}MnO_3$ ($x = 0$, 0.05 and 0.1) samples were synthesized by the sol–gel process. Using a phenomenological model, we have simulated the magnetic and magnetocaloric data as a function of temperature under different applied magnetic fields up to 5 T. The good agreement obtained confirms that our samples exhibit a second-order PM–FM transition when temperature decreases. The theoretical RCP values under an applied magnetic field of 5 T are found to be 196, 186 and 190.5 J kg^{-1} for $x = 0$, 0.05 and 0.1, respectively. Furthermore, the heat capacity values are also high compared to other manganites. The advantage of this method is that we can predict ΔS_M, RCP and the heat capacity values to evaluate the efficiency of several compounds for magnetic refrigeration. Particularly, our studied compounds are shown to be efficient for magnetic refrigeration at low temperatures.

Acknowledgements

This work has been supported by the Tunisian Ministry of Higher Education and Scientific Research.

References

[1] Phong P T, Dang N V, Nam P H, Phong L T H, Manh D H, An N M *et al* 2016 *J. Alloys Compd.* **683** 67
[2] Mira J, Rivas J, Hueso L E, Rivadulla F and Lopez Quintela M A 2002 *J. Appl. Phys.* **91** 8903
[3] Wang Z, Xu Q, Sun J, Pan J and Zhang H 2011 *Phys. B* **406** 1436
[4] Gschneidner Jr K A, Pecharsky V K and Tsokol A O 2005 *Rep. Prog. Phys.* **68** 1479
[5] Zheng X, Zhang B, Li Y, Wu H, Zhang H, Zhang J *et al* 2016 *J. Alloys Compd.* **680** 617
[6] Pecharsky V K and Gschneidner K A 1997 *Phys. Rev. Lett.* **78** 4494
[7] Hu F-X, Shen B-G, Sun J-R, Cheng Z-H, Rao G-H and Zhang X-X 2001 *Appl. Phys. Lett.* **78** 3675

[8] Zheng X Q, Shao X P, Chen J, Xu Z Y, Hu F X, Sun J R *et al* 2013 *Appl. Phys. Lett.* **102** 022421
[9] Phan M H and Yu S C 2007 *J. Magn. Magn. Mater.* **308** 325
[10] Ben Jazia Kharrat A, Hlil E K and Boujelben W 2018 *J. Alloys Compd.* **739** 101
[11] Krichene A, Bourouina M, Venkateshwarlu D, Solanki P S, Rayaprol S, Ganesan V *et al* 2016 *J. Magn. Magn. Mater.* **408** 116
[12] Krichene A, Solanki P S, Rayaprol S, Ganesan V, Boujelben W and Kuberkar D G 2015 *Ceram. Int.* **41** 2637
[13] Hamad M A 2014 *Phase Transit.* **87** 460
[14] Hamad M A 2015 *J. Adv. Ceram.* **206** 210
[15] Gharsallah H, Bejar M, Dhahri E, Hlil E K and Bessais L 2016 *Ceram. Int.* **42** 697
[16] Hsini M, Hcini S and Zemni S 2018 *J. Magn. Magn. Mater.* **466** 368
[17] Bingham N S, Phan M H, Srikanth H, Torija M A and Leighton C 2009 *J. Appl. Phys.* **106** 023909
[18] Ben Jazia Kharrat A, Moussa S, Moutiaa N, Khirouni K and Boujelben W 2017 *J. Alloys Compd.* **724** 389
[19] Hamad M A 2014 *Phase Transit.* **85** 460
[20] Hamad M A 2012 *Mater. Lett.* **82** 181
[21] Hamad M A 2012 *Phase Transit.* **85** 106
[22] Zhong W, Chen W, Ding W P, Zhang N, Hu A, Du Y W and Yan Q J 1998 *Eur. Phys. J. B* **3** 169
[23] Dhahri A H, Jemmali M, Dhahri E and Valente M A 2015 *J. Alloys Compd.* **638** 221
[24] Zener C 1951 *Phys. Rev.* **81** 440
[25] Guo Z B, Du Y W, Zhu J S, Huang H, Ding W P and Feng D 1997 *Phys. Rev. Lett.* **78** 1142
[26] Reis M S, Amaral V S, Araújo J P, Tavares P B, Gomes A M and Oliveira I S 2005 *Phys. Rev. B* **71** 144413
[27] Dong Q Y, Zhang H W, Sun J R, Shen B G and Franco V 2008 *J. Appl. Phys.* **103** 116101
[28] Franco V, Blázquez J S and Conde A 2006 *Appl. Phys. Lett.* **100** 064307
[29] Franco V and Conde A 2010 *Int. J. Refrig.* **33** 465
[30] Franco V, Conde A, Kuz'min M D and Romero-Enrique J M 2009 *J. Appl. Phys.* **105** 917
[31] Widom B 1965 *J. Chem. Phys.* **43** 3898